AIMS Materials Science, 12(6): 1153–1175.
DOI: 10.3934/matersci.2025054
Received: 08 October 2025
Revised: 09 November 2025
Accepted: 14 November 2025
Published: 28 November 2025

https://www.aimspress.com/journal/Materials

Research article

Comparative study of the mechanical properties of ASA, nylon, and nylon reinforced with carbon fiber components made by 3D printing

Juan Sebastián Ramírez-Prieto, Juan Sebastián Martínez-Yáñez and Andrés Giovanni González-Hernández*

Grupo de Investigación en Desarrollo y Tecnología de Nuevos Materiales (GIMAT), Universidad Industrial de Santander, Carrera 27 calle 9, Bucaramanga, Santander, 680006, Colombia

* **Correspondence:** Email: aggonzal@uis.edu.co; Tel: +60-7-6344000.

Abstract: The mechanical performance of components fabricated via fused deposition modeling (FDM) is critically influenced by both processing parameters and material selection. In this work, a systematic comparison was performed among acrylonitrile styrene acrylate (ASA), polyamide (PA), and carbon fiber-reinforced polyamide (PA-CF) to assess their tensile and flexural responses at three infill densities (33%, 66%, and 100%). Standardized ASTM specimens were printed under controlled conditions, and mechanical testing was complemented with fracture surface inspection to identify failure mechanisms associated with layer adhesion and internal porosity. A statistical analysis based on an analysis of variance (ANOVA) design revealed that both material type and infill density exert significant effects on strength, stiffness, and strain at break, with a strong interaction between the two factors. Increasing infill density consistently enhanced tensile and flexural strengths, although the degree of improvement depended on the intrinsic ductility and interlayer bonding of each polymer. Among the tested materials, PA exhibited the highest tensile and flexural strengths combined with superior ductility, while ASA showed greater stiffness but lower elongation. The PA-CF composite displayed intermediate performance, possibly influenced by the short carbon fibers embedded in the filament, which create local discontinuities within the polymer matrix and reduce overall ductility. These findings provide valuable insights for optimizing FDM parameters to enhance the structural integrity of additively manufactured components.

Keywords: mechanical properties; tensile strength; flexural strength; 3D printing; FDM; ASA; PA; PA-CF

1. Introduction

Additive manufacturing (AM) has fundamentally transformed modern production paradigms by enabling the layer-by-layer fabrication of complex geometries directly from digital models. Among the various AM techniques, fused deposition modeling (FDM) has emerged as one of the most widely adopted methods due to its cost-effectiveness, accessibility, and compatibility with a broad spectrum of thermoplastic materials [1,2]. FDM is an extrusion-based process wherein a thermoplastic filament is fed into a heated nozzle, melted, and deposited along predefined paths to construct parts in a layer-by-layer manner [3]. The slicing of a computer-aided design (CAD) model into cross-sectional layers enables precise control over the geometry and internal structure of the printed object. At the same time, the z-axis motion facilitates the stacking of layers to form the final three-dimensional component [4–6]. This process enables the fabrication of parts with intricate internal and external geometries, eliminating the need for traditional tooling [6]. The main advantages of FDM include low capital investment, rapid prototyping capability, and the availability of diverse polymer feedstocks. However, the technique is also subject to intrinsic limitations, such as anisotropic mechanical behavior resulting from the sequential deposition of layers, relatively low resolution, and the frequent need for support structures in overhanging regions [7]. These drawbacks become particularly relevant when high structural performance and dimensional accuracy are required. Weak interlayer adhesion and the presence of voids further contribute to diminished strength and stiffness along the build (Z) direction [8]. Consequently, enhancing the mechanical performance of FDM polymers remains essential for their broader adoption in functional applications [3,9]. Standardized mechanical testing (ASTM D638 tensile, D790 flexural, and D256 impact specimens) is routinely employed to evaluate these materials, yielding quantitative benchmarks for tensile strength, modulus, and impact resistance [10,11]. Such rigorous assessments not only establish material feasibility for engineering applications but also provide critical data to optimize process parameters and improve part performance. Ultimately, advancing the mechanical reliability of FDM parts—through both material innovation and process refinement—is pivotal for transitioning from prototyping to the fabrication of load-bearing components [9].

Recent advancements in additive manufacturing have led to an in-depth investigation of the mechanical performance of components produced via FDM [12], with a particular focus on engineering-grade polymers such as acrylonitrile styrene acrylate (ASA) [13,14], polyamide (PA, nylon) [15,16], and carbon fiber-reinforced polyamide (PA-CF) [17–19]. Numerous studies have demonstrated that incorporating short carbon fibers into a nylon matrix substantially improves tensile strength and stiffness compared to unreinforced (neat) nylon [20,21], due to enhanced load transfer mechanisms and increased rigidity of the composite structure [22–24]. Conversely, ASA, valued for its exceptional weatherability and ultraviolet (UV) resistance, has gained traction in applications exposed to outdoor environments [25,26]. Nevertheless, its mechanical properties are highly sensitive to processing parameters, which can lead to significant variations in performance [13,27,28]. A key determinant of the mechanical performance of FDM-fabricated components is the influence of processing parameters [29]. Extensive research has established that variables such as print speed, layer thickness, nozzle temperature, and infill density critically affect the strength, stiffness, and overall durability of the final printed parts. Ahn et al. [5] demonstrated the inherently anisotropic nature of FDM-printed structures, attributing variations in tensile strength to differences in interlayer adhesion resulting from the layer-by-layer deposition process. In a complementary study, Turner et al. [4]

conducted an in-depth analysis of the melt extrusion dynamics, revealing that lower layer heights promote enhanced interlayer fusion, which in turn leads to improved tensile performance. Zisopol et al. observed ASA tensile strength improvements of 30% when optimizing layer height and infill, with ASA outperforming a comparable material (PETG) by roughly 20% in ultimate strength under optimal settings [30]. Moreover, infill density has a pronounced effect on ASA part performance; increasing fill from 50% to 100% can significantly raise tensile strength as the material approaches a solid interior [30]. Beyond strength, a key asset of ASA is its environmental durability: unlike acrylonitrile butadiene styrene (ABS), which embrittles and loses toughness under UV exposure, ASA retains its mechanical properties under prolonged sunlight and weathering [25]. This stability, combined with ASA's relatively low shrinkage and warping, makes it ideal for outdoor engineering applications (e.g., automotive housings) where sustained mechanical performance is required in harsh conditions [25].

Extensive research on nylon-based materials has demonstrated that the mechanical performance of FDM-printed components can be significantly improved through careful optimization of printing parameters. PA, commonly referred to as nylons, are commercially available, moderately priced, non-biodegradable engineering polymers known for their high tensile strength, resilience, and impact resistance [31]. However, their hydrophilic nature presents a key limitation, as moisture absorption can lead to surface imperfections and dimensional instability [31,32]. In the context of additive manufacturing, nylon parts produced via FDM are particularly prone to surface roughness resulting from the staircase effect, warpage, and thermal distortion—defects inherent to the layer-by-layer deposition process [31,32]. Lay et al. [33] conducted a comparative study between nylon parts fabricated via FDM and those produced by injection molding, concluding that although FDM-printed specimens generally exhibit inferior mechanical properties, this gap can be partially bridged through precise control of key parameters such as nozzle temperature and infill density. Further insights were provided by Ramesh and Panneerselvam [34], who systematically analyzed the mechanical behavior of FDM-printed nylon components. Their findings revealed that infill density is the most influential parameter affecting tensile strength, flexural strength, impact resistance, and Shore D hardness. Moreover, the combined optimization of high infill density, reduced layer height, and controlled print speed resulted in significant improvements across all evaluated properties. The study also highlighted the effectiveness of statistical tools, such as the Taguchi method and ANOVA, in identifying optimal process conditions, thereby reinforcing their value in the context of additive manufacturing process optimization [34]. More recently, Gonabadi et al. [35] proposed an experimental–numerical approach combining mechanical testing, digital image correlation, and finite-element analysis to characterize FDM-printed short fiber–reinforced polyamide composites. Their results showed strong agreement between simulations and experiments, confirming that carbon fiber-reinforced PA offers superior stiffness-to-weight performance compared to glass fiber composites [35]. Complementary to these findings, Gonabadi et al. [36] developed a hybrid nano-indentation and finite-element homogenization framework to determine the orthotropic properties of 3D-printed fiber-reinforced composites. This approach accurately captured the elastic, plastic, and visco-plastic responses of polyamide matrices while reducing experimental effort and improving the prediction of stress transfer and stiffness anisotropy [36]. These advanced experimental and numerical methodologies have strengthened the understanding of how microstructural parameters—such as fiber orientation, interfacial bonding, and matrix viscoelasticity—govern the macroscopic mechanical behavior of additively manufactured composites.

In the case of carbon fiber–reinforced nylon, Tekinalp et al. [37] reported that the incorporation of short carbon fibers markedly enhances both stiffness and tensile modulus. However, these mechanical gains may be accompanied by reduced interlayer adhesion, a consequence of the intrinsic brittleness and limited ductility of the fiber reinforcements, which can inhibit effective fusion between printed layers. In another investigation, Gómez-Ortega et al. [38] systematically assessed print parameters: wall thickness, infill density, and nozzle temperature, together with their effects on porosity and interlayer fusion in PA6/66-carbon fiber composites produced by FDM. Employing a Taguchi L9 design, they demonstrated that although a 99% infill delivers the highest tensile (52.8 MPa) and flexural (67.4 MPa) strengths, the optimal trade-off among stiffness, strength, and toughness is achieved with a 66% infill, 1.2 mm wall thickness, and a 255 °C nozzle setting. This configuration demonstrates that near-peak mechanical performance can be maintained while significantly reducing material usage, rather than relying on fully dense (100%) prints. In another study on carbon fiber–reinforced nylon, Matsika Klossa et al. (2023) [39] investigated the influence of chopped carbon fiber content (0%–20 wt.%) and raster orientation (0°, ±45°, 90°) on the tensile properties of FDM-printed specimens. Their results revealed that while pure nylon exhibited relatively consistent mechanical behavior regardless of raster angle, the addition of carbon fibers introduced a strong anisotropy: specimens with 10 wt.% reinforcement printed at 0° showed the highest tensile strength and Young's modulus. This orientation aligns the short fibers with the tensile load, maximizing stress transfer. Furthermore, a finite element analysis of a transtibial patellar tendon bearing (PTB) socket using the optimal composite confirmed that the stresses remained within the elastic region under typical physiological loading conditions. These findings highlight the viability of moderately reinforced nylon composites for structural applications in personalized medical devices produced via additive manufacturing. In another study, Rodríguez-Reyna et al. [40] explored the optimization of mechanical properties in 3D-printed parts made from polylactic acid (PLA), ABS, and carbon fiber–reinforced nylon (N + CF) using FDM technology. Through a two-factorial design of experiments (DOEs), the authors rigorously evaluated the effects of key printing parameters, including infill percentage, raster orientation, layer thickness, and geometric pattern, on ultimate tensile strength (UTS) and Young's modulus. Notably, the study demonstrated that UTS can surpass that of the original filament in both PLA and N + CF when optimal conditions are applied, particularly at 100% infill, reduced layer thickness (0.14 mm), and a +45°/–45° deposition angle [40]. The research further establishes a strong correlation ($R^2 > 0.94$) between specimen density and UTS, underscoring the role of material densification in enhancing mechanical properties [40]. In another work, Dubey et al. [41] examined five distinct infill patterns (grid, triangular, sinusoidal, honeycomb, and rectilinear) and evaluated their influence on the mechanical, thermal, and microstructural behavior of short carbon fiber–reinforced nylon composites produced via FDM. Through tensile and flexural testing, the authors demonstrated that the rectilinear pattern achieved the highest ultimate tensile strength (34.58 MPa) and stiffness (Young's modulus = 982 MPa). In comparison, the triangular pattern delivered superior flexural strength (23.45 MPa) and the greatest dynamic storage moduli in both tensile (747 MPa) and flexural (1280 MPa) dynamic mechanical analysis tests [41]. These results highlight the crucial role of infill geometry in enhancing load transfer, energy dissipation, and dimensional accuracy for high-performance, additively manufactured composite components [41].

Despite this progress, several challenges and knowledge gaps remain in comparing and optimizing ASA, nylon, and CF-nylon for FDM. One central challenge is the pronounced influence of processing conditions on mechanical outcomes for each material. Print orientation, layer thickness,

raster angle, and annealing conditions can all substantially alter tensile and flexural properties [8]. For example, changing the build orientation from flat to upright can reduce the tensile strength of FDM polymers by 30%–50% due to the layered structure [8]. Nylon and ASA parts each respond differently to such parameters: nylon tends to require higher temperatures and slower speeds to ensure interlayer diffusion, whereas ASA (an amorphous polymer) is less sensitive to cooling rates but can suffer from residual stresses if not printed with an adequate enclosure [31,42]. The current literature lacks a systematic, head-to-head comparison of these materials under identical print settings; most studies optimize parameters for one material at a time, making it difficult to isolate inherent material differences from processing effects. Another issue is material anisotropy and the underlying structure–property relationships. While it is known that all FDM parts are anisotropic, the degree and nature of anisotropy differ between ASA, PA, and CF-PA [8].

Addressing these challenges, there is a clear rationale for a focused comparative study of ASA, PA, and PA-CF in FDM. Such a study fills critical research gaps and provides valuable guidelines for both researchers and practitioners. It establishes a reference baseline of mechanical performance—specifically tensile strength and flexural modulus—for each material under identical specimen geometry and printing parameters. This standardization enables a direct, like-for-like comparison that is currently absent from the literature. Moreover, it facilitates material selection; for instance, when carbon fiber–reinforced nylon exhibits superior tensile strength compared to ASA but markedly lower impact toughness, engineers can make informed decisions depending on whether stiffness or impact resistance is prioritized in the design. By using standard test specimens (e.g., ASTM D638 Type IV tensile samples, D790 flexural samples) printed with the same infill and orientation for all three materials, the study ensures that observed differences are intrinsic to the material compositions themselves.

Based on the foregoing, this study examines the influence of infill percentage and material type on the tensile strength, flexural strength, and elastic modulus of FDM-printed specimens. Three materials were selected–ASA, PA, and PA-CF–in combination with three infill levels: 33%, 66%, and 100%. To systematically evaluate these factors, an n^k factorial experimental design was employed, comprising 45 specimens for tensile testing and an additional 45 specimens for flexural testing.

2. Materials and methods

All filaments employed in this work were eSUN commercial filaments with diameters of 1.75 mm. The nominal properties reported by the manufacturer are summarized in Table 1. In particular, the PA-CF filament consists of a polyamide-6 (PA6) matrix (75–85 wt.%) reinforced with 15–20 wt.% short carbon fibers and 2–5 wt.% additives. Nevertheless, a noticeable divergence was observed between the manufacturer's specifications and the experimental values obtained in this study, in line with the discrepancies previously reported by Calignano [9]. It is also important to note that the mechanical properties reported for the as-supplied filament correspond to those of a single fiber, whereas the mechanical response of a fully 3D-printed component can differ significantly due to the combined effects of process-induced porosity, interlayer adhesion, and fiber orientation.

The 3D printer used to fabricate the specimens was a FlashForge Guider 3 (Figure 1). Tensile and flexural tests were conducted using a Tinius Olsen universal testing machine H25KS, with a capacity of 25 kN.

Table 1. 3D filament properties according to manufacturers.

Mechanical properties	ASA	PA	PA-CF
Density (g/cm^3)	1	1.12	1.24
Elongation (%)	30	175.32	10.61
Young's modulus (MPa)	4300	1370	4363
Ultimate tensile strength (MPa)	50	52.45	140
Ultimate flexural strength (MPa)	35	58	140

Figure 1. General view of the FlashForge Guider 3 3D Printer, showing the main elements.

Table 2 summarizes the mechanical testing parameters employed in this study. For tensile testing, the tensile speed and grip separation were selected in accordance with ASTM D638 recommendations, ensuring reliable strain-rate control and reproducibility of specimen elongation. Flexural testing was conducted in accordance with ASTM D790 guidelines, utilizing well-defined support spans and loading rates to accurately capture the bending response of the printed polymers. Distinct testing speeds were applied for tensile evaluation of each material (0.5 mm/min for ASA, 15 mm/min for PA, and 5 mm/min for PA-CF), reflecting preliminary adjustments aimed at preventing premature failure or slippage while maintaining comparability across tests. These adjustments were implemented to ensure that the total duration of the tensile tests remained within the specified range of 0.5–5 min, as outlined in ASTM D638. For the flexural tests, the loading speed and support span were defined in accordance with ASTM D790, which establishes the relationship between specimen thickness and the span-to-depth ratio to ensure reliable bending results. A constant flexural speed of 2 mm/min was employed for ASA specimens. In comparison, a higher rate of 4 mm/min was used for PA and PA-CF, reflecting the greater ductility and load-bearing capacity of these materials. Similarly, the support span was adjusted to 70 mm for ASA and 40 mm for PA and PA-CF, thereby maintaining the recommended span-to-thickness ratio and preventing non-standard failure modes (shear or local indentation). These conditions ensured that the flexural response was representative of each material's intrinsic mechanical behavior, allowing for consistent comparisons across the different 3D-printed parts.

Table 2. Testing parameters.

	Tensile speed (mm/min)	Grip distance (mm)	Flexural speed (mm/min)	Support distance (mm)
ASA	0.5	68	2	70
PA	15	68	4	40
PA-CF	5	68	4	40

The specimens were modeled using Autodesk Fusion 360 CAD software. Flexural specimens were designed in accordance with ASTM D790, adopting rectangular geometry with dimensions of 127 mm in length, 12.7 mm in width, and 3.2 mm in thickness, which satisfy the span-to-depth ratio requirements specified by the standard. Tensile specimens were modeled following the Type IV geometry prescribed by ASTM D638, as illustrated in Figure 2. This configuration is commonly used for polymer testing, with a thickness of 3.2 mm and a reduced section designed to promote uniform stress distribution during tensile loading.

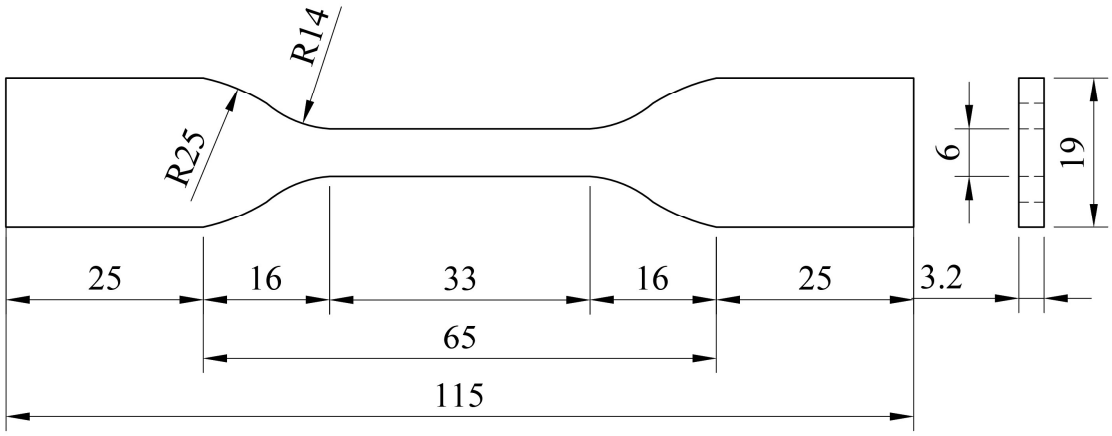

Figure 2. Geometry and dimensions of the tensile test specimen (units in mm) according to ASTM D638 Type IV standard.

The elastic modulus was determined following the procedure described in ASTM D638-22 by calculating the slope of the initial linear region of the stress–strain curve. The yield strength was determined using the 0.2% offset method, in which a line parallel to the elastic portion of the curve, displaced by 0.002 units of strain, was drawn, and its intersection with the experimental curve was taken as the yield point, following Annex A1 and A2 of ASTM D638. The percent elongation at break was obtained by measuring the extension of the specimen at the point of rupture, dividing that extension by the original gauge length, and multiplying the result by 100. As specified by ASTM D638-22 for Type IV specimens, the gauge length used in this study was 25 mm, ensuring standardization and comparability of the mechanical results. The flexural strength (σ_f) and flexural modulus (E_B) of the specimens were determined in accordance with the procedures described in the ASTM D790 standard. Both parameters were calculated using Eqs 1 and 2, which correspond to the standard formulations for three-point bending tests.

$$\sigma_f = \frac{3PL}{2bd^2} \tag{1}$$

$$E_B = \frac{mL^3}{4bd^3} \tag{2}$$

where P is the maximum load (N), L is the support span (mm), b is the width of the beam tested (mm), d is the depth of the beam tested (mm), and m is the slope of the tangent to the initial straight-line portion of the load–deflection curve (N/mm of deflection).

The CAD models were exported in STL (Standard Tessellation Language) format and subsequently processed with the slicer software FlashPrint, provided by the same manufacturer as the 3D printer employed in this study. This workflow ensured precise control over specimen geometry and reproducibility across the different materials and test conditions.

The slicing process was carried out using FlashPrint, which generates output files with the .gx extension, containing the complete set of instructions for extrusion temperature, build platform heating, and toolpath movements. Table 3 summarizes the processing conditions used for each material, which were defined based on manufacturer recommendations, default settings from the FlashPrint software, and complementary data reported in the literature. Once the spools of filament were unsealed, they were immediately used for printing to minimize any exposure to ambient humidity. The drying process was not included as part of the standard pre-printing procedure; however, it was carried out whenever the filament had been exposed to ambient conditions for more than 1 or 2 h, in order to ensure its optimal characteristics during printing and to prevent moisture presence in the filament. Under these conditions, before printing, the PA and PA-CF filaments were dried in a convection oven for 12–14 h at 70 °C, as recommended by the manufacturer. This procedure effectively limited moisture absorption, thereby maintaining stable melt viscosity, improving interlayer adhesion, and ensuring a uniform surface finish. The 3D printing system used in this study (see Figure 1) was equipped with a fully enclosed build chamber, providing a controlled environment that further reduced the influence of ambient humidity and temperature fluctuations on filament stability. These combined measures contributed to enhanced dimensional accuracy and mechanical consistency of the printed components. Extrusion and platform temperatures were set according to the thermal characteristics of each filament: ASA (240/100 °C), PA (265/90 °C), and PA-CF (280/70 °C). Printing speeds ranged from 40 to 60 mm/s to mitigate warping. A uniform layer height of 0.2 mm was selected for all specimens, ensuring consistent surface finish and interlayer adhesion. Linear infill patterns were adopted with a raster angle of 90°/90°, which provides a balanced distribution of stresses along orthogonal directions. Infill density was incorporated as a key variable in the experimental design, with three levels selected (33%, 66%, and 100%) to analyze the effect of internal architecture on mechanical performance. Extrusion and platform temperatures, as well as printing speeds, were individually adjusted for each polymer to achieve stable extrusion flow and proper interlayer bonding, following the manufacturer's recommendations. Nevertheless, such variations can influence the resulting microstructure and, therefore, the mechanical response of the printed parts. Differences in thermal profiles may alter interlayer diffusion, residual stress relaxation, and crystallization behavior, particularly in semicrystalline materials such as PA and PA-CF. Consequently, part of the variability observed in tensile and flexural performance may arise not only from intrinsic material characteristics but also from these processing-related effects. Even maintaining the recommended conditions ensured adequate printability and reproducibility across all samples, allowing for a representative comparison under practical printing conditions and the exact structure of the samples.

Table 3. 3D printing parameters by material.

3D printing parameters	ASA	PA	PA-CF
Extruder temperature (°C)	240	265	280
Platform temperature (°C)	100	90	70
Printing speed (mm/s)	60	40	60
Layer height (mm)	0.2	0.2	0.2
Geometrical pattern (–)	Linear	Linear	Linear
Raster angle (°)	0°/90°	0°/90°	0°/90°
Infill density (%)	33, 66, 100	33, 66, 100	33, 66, 100
Wall line count (Walls)	3	3	3
Top/bottom layers (Layers)	4	4	4
Overlap perimeter (%)	30	30	30

Figure 3 illustrates the infill structures generated by FlashPrint for both flexural (top) and tensile (bottom) specimens at each density level. Lower infill density (33%) resulted in highly porous geometries with reduced material usage. In contrast, intermediate infill density (66%) and full infill density (100%) produced progressively denser structures, directly influencing stiffness, load-bearing capacity, and failure mechanisms.

To systematically evaluate the effect of processing parameters on mechanical performance, a statistical factorial design was employed. Factorial designs facilitate the simultaneous study of multiple variables, reducing variability and enhancing reproducibility. In the classical n^k factorial approach, n denotes the number of levels for each factor, while k represents the number of factors considered. In this work, two factors were analyzed: material type (ASA, PA, and PA-CF) and infill density (33%, 66%, and 100%), resulting in a 32-factorial design comprising 90 experimental runs. Data analysis was performed using Minitab software, enabling efficient statistical treatment and interpretation of the results. The sample nomenclature adopted for this study is illustrated in Figure 4, and the complete factorial scheme is detailed in Table 4.

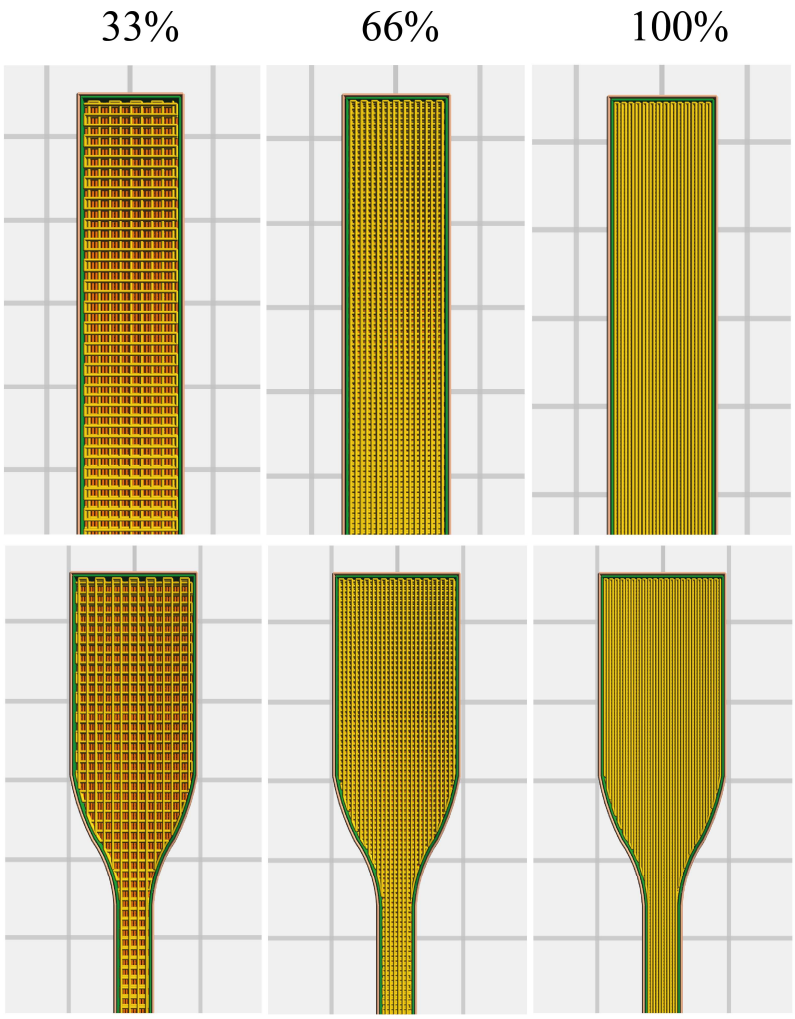

Figure 3. Infill density patterns generated by FlashPrint for specimens at three density levels: 33%, 66%, and 100%. The top row corresponds to flexural specimens and the bottom row to tensile specimens.

Table 4. Design of experiments (DOE).

Material	Infill density (%)	Flexural samples	Tensile samples
ASA	100	AF1-5	AT1-5
	66	AF6-10	AT6-10
	33	AF11-15	AT11-15
PA	100	NF1-5	NT1-5
	66	NF6-10	NT6-10
	33	NF11-15	NT11-15
PA-CF	100	CF1-5	CT1-5
	66	CF6-10	CT6-10
	33	CF11-15	CT11-15

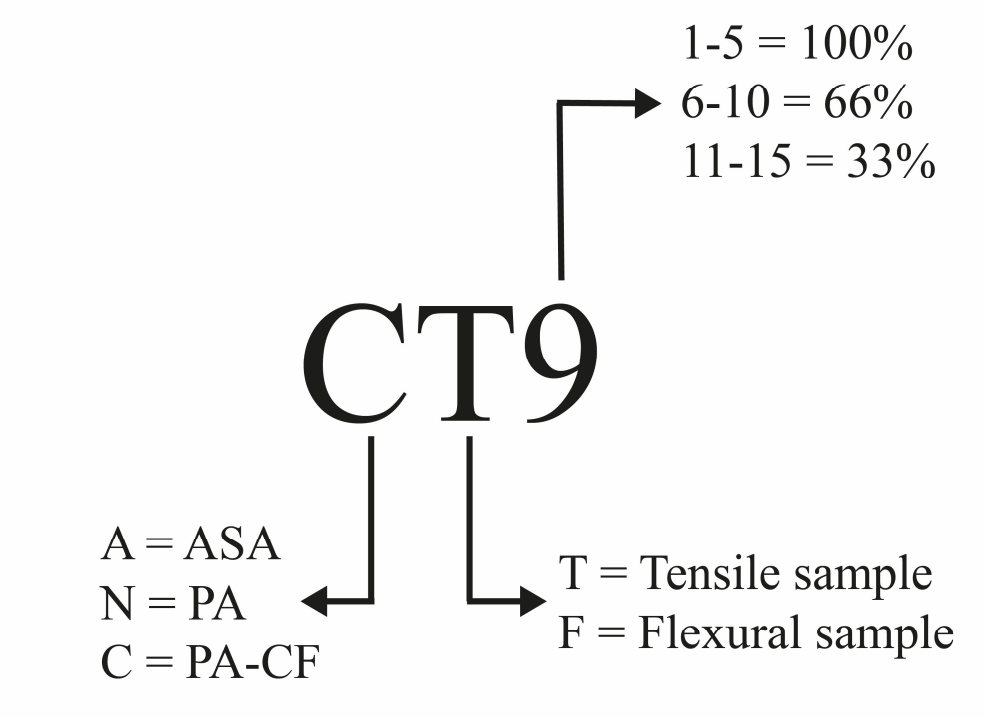

Figure 4. Specimen's nomenclature.

3. Results and discussion

Figure 5 present the stress–strain curves obtained for ASA, PA, and PA-CF specimens manufactured with three distinct infill densities: 100% (red), 66% (green), and 33% (blue). These curves reveal the direct influence of internal architecture on tensile behavior, showing that specimens with higher infill consistently outperform those with reduced densities in both stiffness and UTS. The trend is evident across the three materials analyzed, confirming the importance of infill density as a design parameter in FDM-printed polymers. The average UTS values for fully dense specimens reached 26.92 MPa for ASA, 38.07 MPa for nylon, and 26.44 MPa for carbon fiber–reinforced nylon, underscoring the fact that the interaction between material composition and fill density plays a critical role in defining mechanical performance. This finding highlights how internal porosity reduction translates into improved load-bearing capacity and simultaneously establishes a baseline for comparison between brittle and ductile thermoplastics, as well as fiber-reinforced composites.

The mechanical response of ASA (Figure 5a) reflects the behavior of a brittle polymer. Its curves are dominated by a nearly linear elastic region, where stress increases proportionally with strain, followed by fracture with minimal or almost no plastic deformation. This linear profile indicates that once the elastic limit is surpassed, the material cannot undergo significant plastic accommodation before catastrophic failure. The progressive reduction in UTS with lower infill densities demonstrates that porosity not only decreases stiffness but also accelerates premature failure. Therefore, ASA specimens printed with 33% or 66% infill density exhibit a significantly diminished ability to sustain applied loads compared to those with full density.

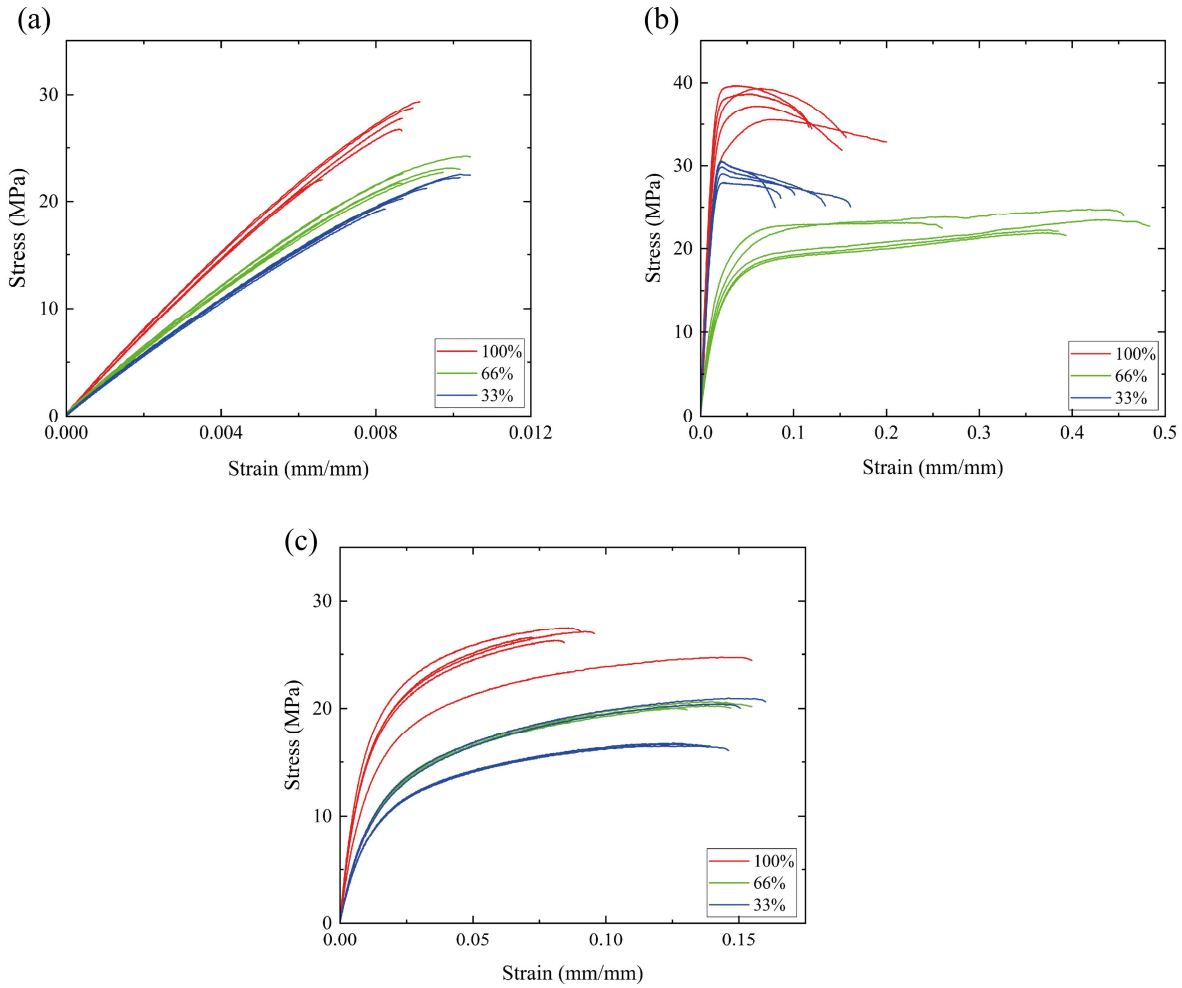

Figure 5. Stress–strain curves obtained from tensile tests of (a) ASA, (b) PA, and (c) PA-CF specimens fabricated with different infill densities.

In contrast, the nylon specimens (Figure 5b) reveal a markedly different stress–strain profile, characteristic of ductile polymers. After an initial linear elastic region, the material yields and enters a broad plastic regime, allowing significant deformation before fracture. This ductility is particularly evident in the 66% infill specimens, which, despite reaching lower maximum stress values than the fully dense samples (100%), exhibit a remarkable capacity for elongation before failure. This behavior may be related to the interaction between the external contour layers and the internal infill pattern: at 66% density, the reduced internal constraint allows the deposited filaments to stretch and accommodate strain more effectively than in the 100% dense specimens, where the higher degree of internal compaction restricts deformation. Consequently, the 66% specimens demonstrate a balance between structural continuity and internal flexibility, providing greater capacity for plastic deformation compared to both 33% and 100% infill densities. These results highlight nylon's superior toughness and its ability to combine moderate strength with enhanced elongation, making it an attractive option for applications that require flexibility, energy absorption, and load-bearing capacity. It is also worth noting that the slightly lower UTS observed for the 66% infill specimens compared to some 33% samples is consistent with the formation of larger internal voids and irregular filament bonding, which hinder effective stress transfer and promote early damage initiation. Additionally, the raster angle configuration employed in this study (ranging from 0 to 90°, as shown in Figure 3) can have a

significant impact on the tensile response. In the 66% infill pattern, the higher frequency of filament crossings increases the number of fiber discontinuities along the loading axis, thereby reducing the effective load transfer through the PA fiber network. Conversely, in the 33% infill specimens, the filament paths are more aligned with the tensile direction, resulting in fewer discontinuities and more efficient stress transmission, which explains their relatively higher UTS than 66% infill.

Figure 5c illustrates the stress–strain curves for PA-CF specimens at different infill densities, highlighting the reinforcing effect of carbon fibers on the tensile response of the polymer matrix. The specimens with 100% infill density exhibit the highest stiffness and ultimate tensile strength, as evidenced by the steep initial slope of the curves and the elevated stress values reached before failure, confirming the efficiency of fiber reinforcement in improving load-bearing capacity. In contrast, reducing the infill density to 66% and 33% results in a progressive decrease in both strength and rigidity, a consequence that can be attributed to the increased porosity of the internal structure and the reduced continuity between filaments, which limits the effective transfer of stress. However, it is noteworthy that some 33% infill specimens display mechanical behavior comparable to that of the 66% group, suggesting that additional factors, such as the anisotropic distribution and orientation of carbon fibers during deposition, as well as the inherent moisture sensitivity of nylon-based composites, influence the reproducibility of the results. These observations are consistent with the trends reported by Muhamedagic et al. [43], who studied a PA6 matrix reinforced with 10 wt.% short carbon fibers and reported higher tensile strengths (~70 MPa). In this work, the filament contained a higher fiber fraction (15–20 wt.%), which also introduced more fiber–matrix interfaces and microstructural discontinuities that can act as stress concentrators, thereby reducing the overall tensile strength. In addition, specimens were printed with a raster angle of 90°, a layer height of 0.2 mm, and a relatively low printing speed, parameters that favor dimensional stability and interlayer adhesion but may also reduce the UTS due to more prolonged exposure to heat and potential microstructural discontinuities. Unlike ASA, which is predominantly brittle, and neat nylon, which exhibits extensive plastic deformation, PA-CF demonstrates an intermediate mechanical response characterized by high tensile strength combined with moderate ductility. This balance between stiffness and deformability not only reduces the risk of sudden catastrophic fracture but also provides a margin of plastic accommodation under load.

Figure 6 shows the representative fracture surfaces of ASA, PA, and PA-CF specimens after tensile testing at different infill densities (100%, 66%, and 33%). Apparent differences in fracture morphology can be observed as a function of both material type and internal architecture. ASA specimens (left column) exhibit well-defined layer boundaries and clean fracture planes, characteristic of brittle failure with limited filament deformation. The reduction in infill density from 100% to 33% reveals an increasingly open internal structure, where interlayer voids become more evident, promoting stress concentration and premature failure, especially in the infill zone.

In contrast, PA specimens (middle column) display extensive plastic deformation and filament stretching, particularly at 66% and 33% infill densities. The fractured surfaces appear rough and irregular, indicating ductile failure and strong bonding between filaments. The large deformation before fracture is consistent with the material's high elongation and energy absorption capacity. For PA-CF specimens (right column), the fracture surfaces appear more compact and uniform than those of neat nylon, with visible fiber reinforcement distributed across the cross-section. At 100% infill, the structure remains dense and cohesive, while lower infill densities reveal internal porosity and partial delamination between layers. The carbon fibers contribute to a stiffer structure and improved load

transfer, but also limit the extent of plastic deformation compared to pure PA. Overall, these microstructural observations support the mechanical trends observed in tensile tests, where PA exhibits the highest ductility, ASA displays the most brittle behavior, and PA-CF shows an intermediate response that combines strength and rigidity. In addition to the stress–strain curves presented in Figure 5, the visual appearance of the fractured specimens is provided in the Supplementary Information (Figures S1–S3), which display representative ASA, PA, and PA-CF samples tested at different infill densities (100%, 66%, and 33%). These supplementary images support the mechanical findings by evidencing the macroscopic patterns associated with material composition.

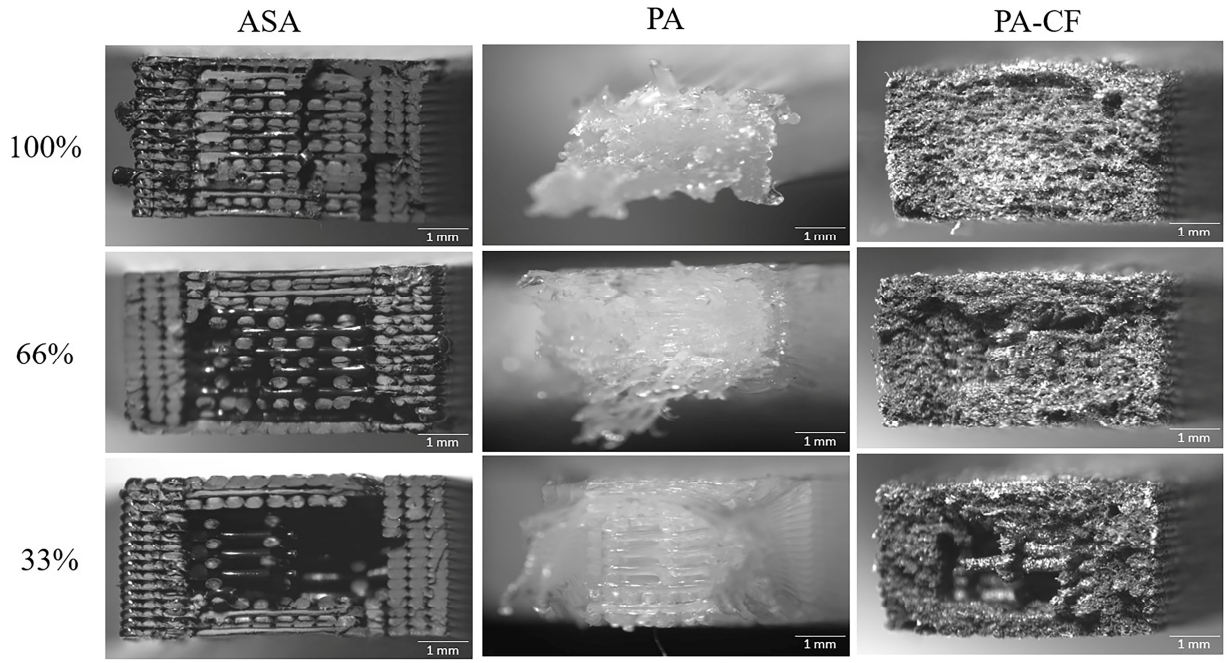

Figure 6. Representative fracture surfaces of ASA, PA, and PA-CF specimens after tensile testing at different infill densities (100%, 66%, and 33%).

Figure 7 presents the load-displacement curves obtained from the three-point bending tests of ASA, PA, and PA-CF specimens fabricated with infill densities of 100%, 66%, and 33%. The results clearly demonstrate that increasing the infill density enhances flexural resistance in all materials, as the fully dense specimens (red curves) consistently sustain higher loads and exhibit steeper initial slopes compared to those with reduced infill densities (green and blue curves). This behavior confirms the direct relationship between internal porosity and the ability of the printed structures to withstand bending stresses. As shown in Figure 7a, ASA specimens with 100% infill density withstand significantly higher tensile forces before failure compared to those printed with 66% and 33% infill densities. The curves exhibit an initial linear region corresponding to elastic behavior, followed by a gradual increase in force until an abrupt fracture occurs. The fully dense samples maintain structural integrity over a wider displacement range, demonstrating superior resistance to bending loads. However, the lack of a plastic deformation stage reflects the brittle character of ASA. Figure 7b (PA) illustrates the flexural response of nylon specimens, which exhibit a distinct peak force followed by a gradual decline, indicative of yielding and plastic deformation, with the test ultimately being stopped due to the large deformations sustained without fracture. In this case as well, none of the specimens

fractured during the tests, and the experiments were terminated after large displacements were achieved. The 100% infill density samples reached the highest maximum load values, while the 66% and 33% infill density specimens displayed lower resistance but demonstrated remarkable elongation. This confirms nylon's capacity to combine toughness with deformation tolerance under bending loads, further emphasizing its ductile behavior and superior ability to absorb energy without fracturing.

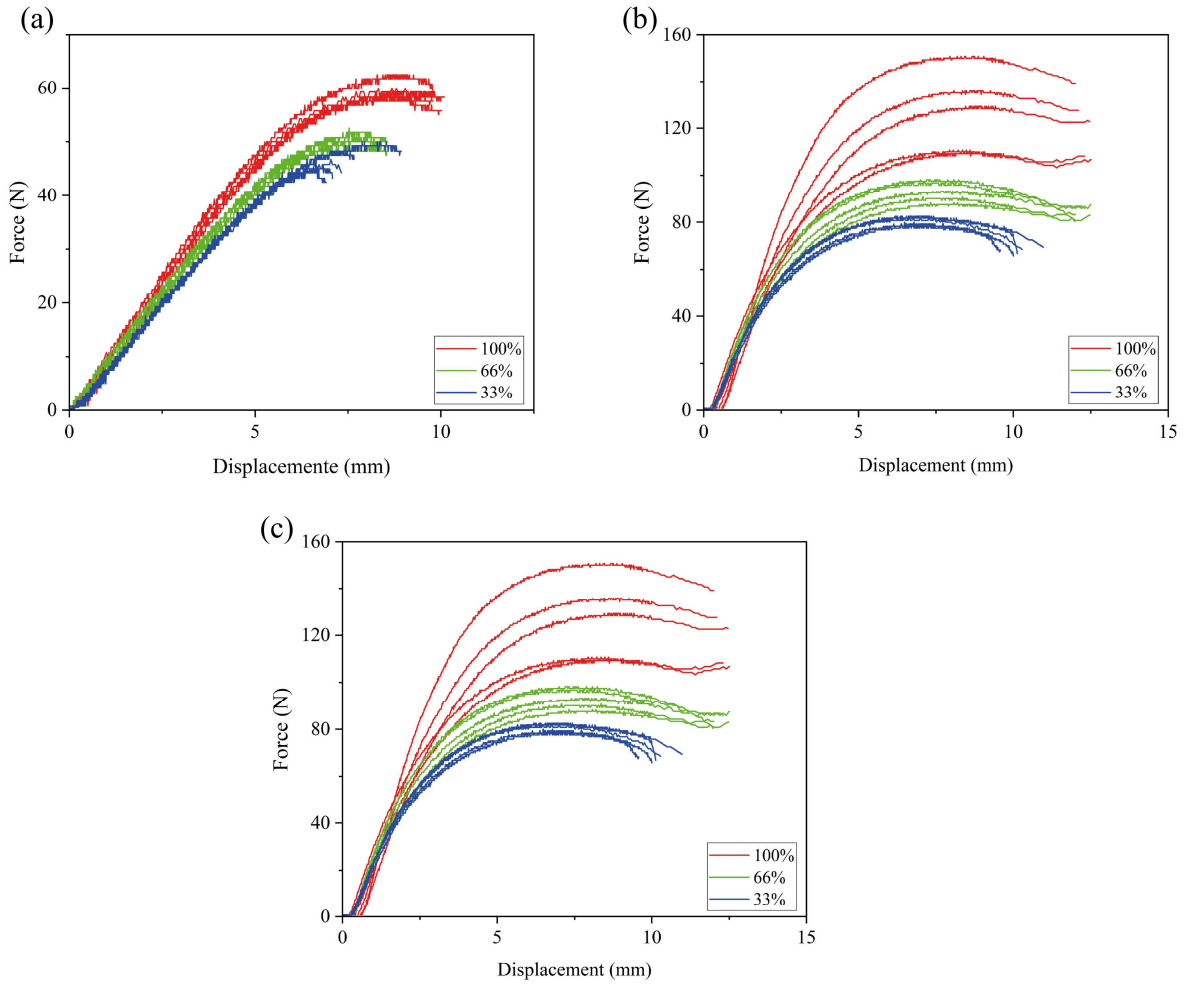

Figure 7. Load-displacement curves obtained from flexural tests of (a) ASA, (b) PA, and (c) PA-CF specimens fabricated with different infill densities.

Figure 7c (PA-CF) demonstrates the reinforcing effect of carbon fibers on the nylon matrix, as the specimens with 100% infill density reached the highest stiffness and load-bearing capacity among the three materials. The steeper initial slope and elevated maximum force confirm the role of fibers in restricting matrix deformation and improving structural performance. As with the PA specimens, the PA-CF specimens did not fracture during the tests; instead, the experiments were stopped after sustained loading, highlighting their ability to deform under bending while retaining structural integrity. At lower infill densities, flexural resistance decreased due to porosity and reduced filament continuity; however, even under these conditions, PA-CF maintained a superior compromise between stiffness and deformation compared to ASA.

Tables 5 and 6 summarize the average mechanical properties obtained from tensile and three-point bending tests for ASA, PA, and PA-CF specimens fabricated with different infill densities.

The results clearly confirm that increasing the infill density enhances the overall mechanical performance. Fully dense specimens (100% infill) consistently exhibited the highest tensile and flexural strengths as well as elastic modulus across all materials. For instance, ASA at 100% infill achieved a tensile strength of 26.9 MPa, a flexural strength of 48.4 MPa, and an elastic modulus of 1920.5 MPa, indicating its stiffness as well as its brittle nature. In addition, the yield strength and elongation at break for ASA were 26.9 MPa and 3.9%, respectively, confirming its limited ductility and tendency toward brittle fracture. PA displayed the best tensile performance, achieving 38.1 MPa in tensile strength (see Table 5) and 71.0 MPa in flexural strength (see Table 6) at 100% infill, values that highlight its superior ductility and load-bearing capacity. Furthermore, the yield strength of PA reached 31.4 MPa, accompanied by an elongation at break of 68.5%, demonstrating a pronounced capacity for plastic deformation before fracture. PA-CF specimens combined high strength with stiffness, as the incorporation of carbon fibers increased the flexural modulus to 1081.1 MPa and flexural strength to 59.1 MPa at full density. However, the PA-CF specimens exhibited a lower tensile strength (UTS) compared to the neat PA samples, showing UTS values more comparable to those of ASA. At 100% infill density, PA-CF reached a tensile strength of 26.4 MPa. In contrast, neat PA achieved a significantly higher value, confirming the superior load-bearing capacity and ductility of the unreinforced polyamide. The tensile strength of PA-CF was nearly equivalent to that of ASA (26.9 MPa), indicating that the incorporation of short carbon fibers did not lead to a substantial improvement in tensile resistance. Moreover, their tensile strength (26.4 MPa), yield strength (12.6 MPa), and elongation at break (45.9%) were notably lower than those of neat nylon (PA), which is likely associated with incomplete stress transfer between the polymer matrix and the short fibers, as well as with fiber discontinuity, interfacial adhesion limitations, and the typical reduction in ductility induced by fiber reinforcement in FDM-processed thermoplastic composites.

Table 5. Tensile properties of ASA, PA, and PA-CF specimens with different infill densities.

Material	Infill density (%)	UTS (MPa)	Tensile modulus (MPa)	Yield strength (MPa)	Elongation at break (%)
SA	100	26.9 ± 2.9	3455 ± 99	26.9 ± 2.9	3.9 ± 0.3
	66	22.9 ± 0.9	2616 ± 79	22.9 ± 0.9	4.4 ± 0.3
	33	21.1 ± 1.4	2390 ± 31	21.1 ± 1.4	4.4 ± 0.3
PA	100	38.1 ± 1.7	2135 ± 96	31.4 ± 3.9	68.5 ± 14
	66	23.1 ± 1.1	662 ± 79	14.2 ± 1.0	181.9 ± 35
	33	29.6 ± 1.1	1860 ± 78	24.7 ± 1.4	51.8 ± 14
PA-CF	100	26.4 ± 1.1	1628 ± 197	12.6 ± 0.7	45.9 ± 13
	66	20.2 ± 0.4	838 ± 78	9.4 ± 1.2	63.2 ± 8
	33	18.2 ± 2.2	835 ± 64	7.6 ± 0.2	66.9 ± 5

Table 6. Flexural properties of ASA, PA, and PA-CF specimens with different infill densities.

Material	Infill density (%)	Flexural strength (MPa)	Flexural modulus (MPa)
ASA	100	48.4 ± 1.3	1920 ± 63
	66	41.0 ± 0.9	1752 ± 58
	33	40.1 ± 4.2	1699 ± 56
PA	100	71.0 ± 3.3	869 ± 47
	66	57.9 ± 6.4	650 ± 114
	33	52.2 ± 1.7	636 ± 138
PA-CF	100	59.1 ± 8.1	1081 ± 54
	66	43.2 ± 2.0	773 ± 35
	33	37.5 ± 0.7	755 ± 48

At reduced infill densities (66% and 33%), all materials showed decreased strength, with values dropping by 10%–30% depending on the property measured. For example, PA specimens at 66% infill exhibited a tensile strength of 23.1 MPa and a flexural strength of 57.9 MPa, while ASA decreased to 22.9 and 41.0 MPa, respectively. Interestingly, PA at 33% infill still achieved a tensile strength of 29.6 MPa, surpassing ASA and PA-CF at the same density. This behavior is also reflected in its yield and elongation values, where PA maintained a yield strength of 24.7 MPa and an elongation at break of 51.8%, highlighting its ability to absorb deformation energy even at lower internal densities. This effect can be attributed to nylon's microstructural characteristics and molecular chain mobility, which enable significant elongation and energy absorption, even when the internal architecture is more porous. In contrast, ASA consistently exhibited brittle behavior, characterized by high stiffness and minimal plastic deformation, with an elongation at break of 4.4% at 33% infill density, confirming its limited capacity for strain accommodation and its tendency toward sudden fracture under tensile loading. On the other hand, PA-CF offered a balanced performance, since the addition of carbon fibers increased both strength and stiffness. Nevertheless, the yield strength and elongation at break decreased to 7.6 MPa and 66.9%, respectively, at 33% infill, reflecting a compromise between rigidity and ductility typical of short-fiber composites.

When comparing the tensile strength of three materials at 100% infill density, nylon (PA) shows the highest performance with an average value of 38.1 MPa. This indicates its superior load-bearing capacity and its ability to withstand higher stresses before failing. In contrast, ASA demonstrates a lower tensile strength of 26.9 MPa, suggesting a more brittle behavior despite its greater stiffness. PA-CF has a tensile strength of 26.4 MPa, which is very close to that of ASA and significantly lower than that of nylon. While incorporating carbon fibers has enhanced stiffness and flexural strength, it has not led to an increase in tensile strength. This may be attributed to factors such as fiber orientation and interfacial bonding within the matrix. Overall, these findings indicate that nylon outperforms both ASA and PA-CF in terms of tensile resistance under fully dense conditions. At the same time, ASA and PA-CF display similar yet lower tensile strength values. Additionally, the tensile modulus values are presented in Table 5, which reveals a clear distinction in stiffness among the tested materials. ASA exhibits the highest tensile modulus, reaching up to 3455 ± 99 MPa at 100% infill, which reflects its inherently rigid amorphous structure and strong interlayer bonding during FDM printing. In contrast, PA and PA-CF specimens show significantly lower modulus values, consistent with the semi-crystalline and more ductile nature of polyamide matrices. Although the incorporation of short carbon fibers in

PA-CF slightly increases stiffness compared to neat PA—owing to the reinforcing effect of the fibers—the improvement is limited by the discontinuous fiber distribution typical of FDM-processed composites. In Table 5, the yield strength and elongation values reveal distinct deformation behaviors among the materials. ASA exhibited a yield strength of 26.9 MPa with a very low elongation of 3.9%, confirming its brittle response at 100% infill. In contrast, PA combined a yield strength of 31.4 MPa with a remarkably high elongation of 68.5%, demonstrating superior ductility. Meanwhile, PA-CF showed intermediate behavior, with a yield strength of 12.6 MPa and an elongation of 45.9%, indicating that carbon fiber reinforcement enhanced stiffness but reduced the material's plastic deformability.

Figure 8 shows the Pareto charts of standardized effects for the two main responses analyzed: (a) UTS and (b) flexural strength. Factor A corresponds to the material type, factor B to the infill density, and AB represents the interaction between both factors. The red vertical line at 2.03 on the x-axis marks the limit for statistical significance at a 95% confidence level ($\alpha = 0.05$). Any factor or interaction whose standardized effect exceeds this limit is considered statistically significant. For UTS (Figure 8a), both material and infill density have a significant impact, with standardized effects exceeding the threshold. The material factor (A) has the most important influence, followed closely by infill density (B). Their interaction (AB) also has a notable contribution, but to a lesser degree. This result shows that the choice of material is the most critical factor in determining tensile strength. However, the internal structure (infill density) and its interaction with material choice also play a role. In contrast, for flexural strength (Figure 8b), the interaction effect (AB) is much smaller, although still statistically significant, suggesting that flexural performance is more directly governed by the intrinsic properties of the material and the degree of infill, with less dependence on their combined interaction.

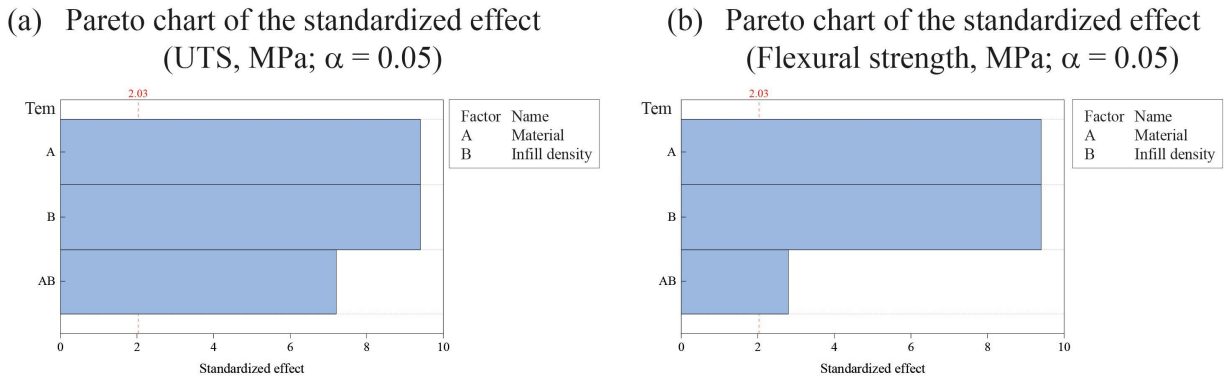

Figure 8. Pareto charts of the standardized effects for (a) UTS and (b) flexural strength of 3D-printed specimens. Factor A: material type; Factor B: infill density.

Figure 9 shows the interaction plots for UTS and flexural strength as they relate to material type and infill density. This highlights how these two factors, when combined, affect the mechanical response of the printed specimens. In terms of tensile behavior (Figure 9a), PA had the highest strength, reaching 38.1 MPa at 100% infill. ASA and PA-CF had similar values around 27 MPa. Notably, even with lower infill densities, PA maintained higher tensile strength than the other two materials, with 29.6 MPa at 33% infill. This demonstrates its ability to withstand tensile loads despite having a higher porosity. In contrast, ASA and PA-CF experienced a greater decrease in tensile performance with lower infill, indicating that their internal structure is more sensitive to changes. For flexural strength (Figure 9b), the effects of both material and infill density were more apparent. Nylon again

had the highest resistance, peaking at 71.0 MPa for 100% infill, followed by PA-CF at 59.1 MPa and ASA at 48.4 MPa. The effect of infill density was especially significant in flexural loading, as strength dropped sharply at 66% and 33% for all materials.

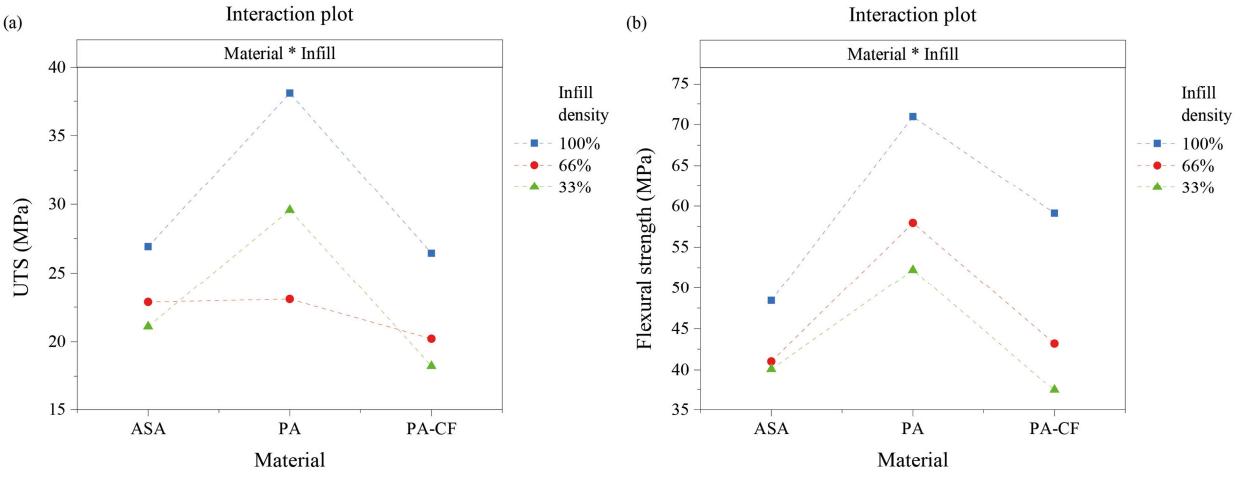

Figure 9. Interaction plot for the factorial design showing the effect of material and infill density on (a) ultimate tensile strength and (b) flexural strength.

4. Conclusions

This work demonstrated the significant influence of both material type and infill density on the tensile and flexural performance of FDM-printed parts made of ASA, PA, and PA-CF using a 2^3 complete factorial design. The experimental results confirm that increasing the infill density improves tensile strength, flexural strength, and elastic modulus across all tested materials. Fully dense specimens (100% infill) consistently outperformed those printed at 66% and 33% densities, indicating the direct contribution of internal architecture (infill density) to load-bearing capacity and stiffness.

Among the studied materials, PA exhibited the best overall performance, achieving the highest tensile strength (38.1 MPa) and flexural strength (71 MPa) at a 100% infill ratio. Even at reduced infill densities, PA retained relatively high tensile properties (29.6 MPa at 33% infill), confirming its superior ability to sustain loads and undergo large deformations without fracture. ASA, by contrast, showed the lowest tensile and flexural strengths, although it maintained the highest elastic modulus (1920 MPa at 100% infill), reflecting its stiff but brittle character. Carbon fiber-reinforced nylon (PA-CF) displayed intermediate behavior: although its tensile strength (26.4 MPa at 100% infill) was comparable to ASA, the addition of carbon fibers and its nylon matrix significantly enhanced flexural strength (59.1 MPa) and stiffness (1081 MPa), providing a favorable balance between rigidity and moderate ductility.

The statistical analysis further confirmed that material selection is the dominant factor influencing both tensile and flexural responses, followed by infill density, with their interaction being particularly relevant for tensile strength. The interaction plots revealed that tensile properties are more sensitive to the combined effect of material and infill, whereas flexural properties are more strongly governed by independent contributions of each factor.

In summary, nylon proved to be the most suitable material for applications requiring high strength and ductility. ASA is more appropriate where stiffness is prioritized, despite its limited toughness.

PA-CF offers a robust compromise between strength and stiffness, owing to fiber reinforcement. These findings provide valuable guidelines for material and design selection in additive manufacturing, where the choice of polymer and internal architecture can be tailored to meet the mechanical demands of specific engineering applications.

Use of AI tools declaration

The authors declare they have not used Artificial Intelligence (AI) tools in the creation of this article.

Author contributions

Andres Giovanni González: conceptualization, methodology, software, formal analysis, investigation, data curation, original draft, writing, review, editing, visualization, supervision; Juan Sebastián Ramirez and Juan Sebastián Martinez: conceptualization, methodology, validation, resources, review.

Acknowledgments

The authors are grateful to the Vice-Rector's Office of Research and Extension (VIE) of the Universidad Industrial de Santander for funding project number 4245 as part of the UIS research challenges and agendas call under the category of Applied Research or Experimental Development for 2024.

Conflict of interest

The authors declare no conflict of interest.

References

1. Ngo TD, Kashani A, Imbalzano G, et al. (2018) Additive manufacturing (3D printing): A review of materials, methods, applications, and challenges. *Compos Part B Eng* 143: 172–196. https://doi.org/10.1016/j.compositesb.2018.02.012
2. Dey A, Roan Eagle IN, Yodo N (2021) A review on filament materials for fused filament fabrication. *J Manuf Mater Process* 5: 69. https://doi.org/10.3390/jmmp5030069
3. Fang Q, Yu J, Shi B (2025) Modelling and optimisation of FDM-printed short carbon fibre-reinforced nylon using CCF and RSM. *Polymers* 17: 1872. https://doi.org/10.3390/polym17131872
4. Turner BN, Strong R, Gold SA (2014) A review of melt extrusion additive manufacturing processes: I. Process design and modeling. *Rapid Prototyp J* 20: 192–204. https://doi.org/10.1108/rpj-01-2013-0012
5. Ahn SH, Montero M, Odell D, et al. (2002) Anisotropic material properties of fused deposition modeling ABS. *Rapid Prototyp J* 8: 248–257. https://doi.org/10.1108/13552540210441166

6. Gao W, Zhang Y, Ramanujan D, et al. (2015) The status, challenges, and future of additive manufacturing in engineering. *Comput-Aided Des* 69: 65–89. https://doi.org/10.1016/j.cad.2015.04.001
7. Syrylbayeva D, Zharylkassyn B, Seisekulova A, et al. (2021) Optimization of the warpage of fused deposition modeling parts using finite element method. *Polymers* 13: 3849. https://doi.org/10.3390/polym13213849
8. Zodhi N, Yang R (2021) Material anisotropy in additively manufactured polymers and polymer composites: A review. *Polymers* 13: 3368. https://doi.org/10.3390/polym13193368
9. Calignano F, Lorusso M, Roppolo I, et al. (2020) Investigation of the mechanical properties of carbon fibre-reinforced nylon filament for 3D printing. *Machines* 8: 52. https://doi.org/10.3390/machines8030052
10. Yankin A, Serik G, Danenova S, et al. (2023) Optimization of fatigue performance of FDM ABS and nylon printed parts. *Micromachines* 14: 304. https://doi.org/10.3390/mi14020304
11. Ramirez-Prieto JS, Martínez-Yáñez JS, Gonzalez-Hernandez AG (2025) Effect of raster angle on the tensile and flexural strength of 3D printed PLA+ parts. *AIMS Mater Sci* 12: 363–379. https://doi.org/10.3934/matersci.2025019
12. Sood AK, Chaturvedi V, Datta S, et al. (2011) Optimization of process parameters in fused deposition modeling using weighted principal component analysis. *J Adv Manuf Syst* 10: 241–259. https://doi.org/10.1142/S0219686711002181
13. Raam Kumar S, Sridhar S, Venkatraman R, et al. (2021) Polymer additive manufacturing of ASA structure: Influence of printing parameters on mechanical properties. *Mater Today Proc* 39: 1316–1319. https://doi.org/10.1016/j.matpr.2020.04.500
14. Vidakis N, Petousis M, Michailidis N, et al. (2025) Thermomechanical recyclability of acrylonitrile styrene acrylate (ASA). *Clean Eng Technol* 25: 100925. https://doi.org/10.1016/j.clet.2025.100925
15. Monkova K, Monka PP, Burgerova J, et al. (2025) Investigating the flexural properties of 3D-printed nylon CF12 with respect to the correlation between loading and layering directions. *Polymers* 17: 788. https://doi.org/10.3390/polym17060788
16. Fisher T, Almeida JHS Jr, Falzon BG, et al. (2023) Tension and compression properties of 3D-printed composites: Print orientation and strain rate effects. *Polymers* 15: 1708. https://doi.org/10.3390/polym15071708
17. Rahman MA, Gibbon L, Islam MZ, et al. (2024) Adjustment of mechanical properties of 3D printed continuous carbon fiber-reinforced thermoset composites by print parameter adjustments. *Polymers* 16: 2996. https://doi.org/10.3390/polym16212996
18. Bianchi I, Mancia T, Mignanelli G, et al. (2024) Effect of nozzle wear on mechanical properties of 3D-printed carbon fiber-reinforced polymer parts by material extrusion. *Int J Adv Manuf Technol* 130: 4699–4712. https://doi.org/10.1007/s00170-024-13035-7
19. Zheng H, Zhu S, Chen L, et al. (2025) 3D printing continuous fiber reinforced polymers: a review of material selection, process, and mechanics–function integration for targeted applications. *Polymers* 17: 1601. https://doi.org/10.3390/polym17121601
20. Mohd Radzuan NA, Khalid NN, Foudzi FM, et al. (2023) Mechanical analysis of 3D-printed polyamide composites under different filler loadings. *Polymers* 15: 1846. https://doi.org/10.3390/polym15081846

21. Li L, Liu W, Sun L (2022) Mechanical characterization of 3D-printed continuous carbon fiber-reinforced thermoplastic composites. *Compos Sci Technol* 227: 109618. https://doi.org/10.1016/j.compscitech.2022.109618
22. Ning F, Cong W, Qiu J, et al. (2015) Additive manufacturing of carbon fiber-reinforced thermoplastic composites using fused deposition modeling. *Compos Part B Eng* 80: 369–378. https://doi.org/10.1016/j.compositesb.2015.06.013
23. Alarifi IM (2022) A performance evaluation study of 3D printed nylon/glass fiber and nylon/carbon fiber composite materials. *J Mater Res Technol* 21: 884–892. https://doi.org/10.1016/j.jmrt.2022.09.085
24. Abderrafai Y, Mahdavi MH (2022) Additive manufacturing of short carbon fiber-reinforced polyamide composites by fused filament fabrication: Formulation, manufacturing and characterization. *Mater Design* 214: 110358. https://doi.org/10.1016/j.matdes.2021.110358
25. Sedlak J, Joska Z, Jansky J, et al. (2023) Analysis of the mechanical properties of 3D-printed plastic samples subjected to selected degradation effects. *Materials* 16: 3268. https://doi.org/10.3390/ma16083268
26. Petousis M, Mountakis N, Spyridaki M, et al. (2025) Process optimization of material extrusion additive manufacturing with ASA: Robust design and predictive models for engineering response metrics. *Int J Adv Manuf Technol* 138: 4431–4453. https://doi.org/10.1007/s00170-025-15779-2
27. Abellán-Nebot JV, Gual-Ortí J, Serrano-Mira J, et al. (2025) Assessing FDM-printed thermoplastics for outdoor tactile graphics: Durability and performance analysis. *Proc Inst Mech Eng Part L* https://doi.org/10.1177/14644207251318006
28. Gawali SK, Jain PK (2025) Effect of natural aging on mechanical properties of 3D-printed acrylonitrile styrene acrylate for outdoor applications. *J Mater Eng Perform* 34: 16430–16442. https://doi.org/10.1007/s11665-024-10273-4
29. Sanford LT, Jaafar IH, Seibi A, et al. (2022) Effect of infill angle, build orientation, and void fraction on the tensile strength and fracture of 3D-printed parts. *Manuf Lett* 33: 569–573. https://doi.org/10.1016/j.mfglet.2022.04.003
30. Zisopol DG, Minescu M, Iacob DV (2024) A study on the influence of FDM parameters on the tensile behavior of samples made of ASA. *Eng Technol Appl Sci Res* 14: 15975–15980. https://doi.org/10.48084/etasr.8023
31. Amithesh SR, Shanmugasundaram B, Kamath S, et al. (2024) Analysis of dimensional quality in FDM-printed nylon 6 parts. *Prog Addit Manuf* 9: 1225–1238. https://doi.org/10.1007/s40964-023-00515-7
32. Farina I, Singh N, Colangelo F, et al. (2019) High-performance nylon 6 sustainable filaments for additive manufacturing. *Materials* 12: 3955. https://doi.org/10.3390/ma12233955
33. Lay M, Thajudin NLN, Hamid ZAA, et al. (2019) Comparison of physical and mechanical properties of PLA, ABS, and nylon 6 fabricated using fused deposition modeling and injection molding. *Compos Part B Eng* 176: 107341. https://doi.org/10.1016/j.compositesb.2019.107341
34. Ramesh M, Panneerselvam K (2021) Mechanical investigation and optimization of parameter selection for nylon material processed by FDM. *Mater Today Proc* 46: 9303–9307. https://doi.org/10.1016/j.matpr.2020.02.697
35. Gonabadi H, Hosseini SF, Chen Y, et al. (2024), Structural analysis of small-scale 3D printed composite tidal turbine blades. *Ocean Eng* 306: 118057. https://doi.org/10.1016/j.oceaneng.2024.118057

36. Gonabadi H, Zamani Miandashti Z, Oila A (2025) Micro-mechanical characterisation of 3D-printed composites via nano-indentation and finite-element homogenization techniques: Overcoming challenges in orthotropic property measurement. *Prog Addit Manuf* 10: 8465–8488. https://doi.org/10.1007/s40964-025-01131-3
37. Tekinalp HL, Kunc V, Velez-Garcia GM, et al. (2014) Highly oriented carbon fiber–polymer composites via additive manufacturing. *Compos Sci Technol* 105: 144–150. https://doi.org/10.1016/j.compscitech.2014.10.009
38. Gómez-Ortega A, Piedra S, Mondragón-Rodríguez GC, et al. (2024) Dependence of the mechanical properties of nylon–carbon fiber composite on the FDM printing parameters. *Compos Part A* 186: 108419. https://doi.org/10.1016/j.compositesa.2024.108419
39. Matsika Klossa C, Chatzidai N, Karalekas D (2023) Tensile properties of 3D-printed carbon fiber-reinforced nylon specimens. *Mater Today Proc* 93: 571–574. https://doi.org/10.1016/j.matpr.2023.02.107
40. Rodríguez-Maya SL, Mata C, Díaz-Aguileta JH, et al. (2022) Mechanical properties optimization for PLA, ABS and nylon + CF manufactured by 3D FDM printing. *Mater Today Commun* 33: 104774. https://doi.org/10.1016/j.mtcomm.2022.104774
41. Dubey D, Singh SP, Behera BK (2025) Mechanical, thermal, and microstructural analysis of 3D-printed short carbon fiber-reinforced nylon composites across diverse infill patterns. *Prog Addit Manuf* 10: 1671–1689. https://doi.org/10.1007/s40964-024-00731-9
42. Gong H, Runzi M, Wang Z, et al. (2025) Influence of filament moisture on 3D printing nylon. *Technologies* 13: 376. https://doi.org/10.3390/technologies13080376
43. Muhamedagic K, Berus L, Potocnik D, et al. (2022) Effect of process parameters on tensile strength of FDM printed carbon fiber reinforced polyamide parts. *Appl Sci* 12: 6028. https://doi.org/10.3390/app12126028

AIMS Press